

BOEING

SCIENTIFIC RESEARCH LABORATORIES

AD 666593

Scattering from Rough Surfaces for Finite Distances Between Transmitter and Receiver

Petr Beckmann

DDC
MAR 26 1958
RECEIVED
A

Reproduced by the
CLEARINGHOUSE
for Federal Scientific & Technical
Information Springfield Va. 22151

This document has been approved
for public release and sale; its
distribution is unlimited.

D1-82-0657

SCATTERING FROM ROUGH SURFACES FOR FINITE DISTANCES
BETWEEN TRANSMITTER AND RECEIVER

by

Petr Beckmann*

Department of Electrical Engineering
University of Colorado
Boulder, Colorado 80302

October 1967

*Consultant:

Geo-Astrophysics Laboratory
Boeing Scientific Research Laboratories
Seattle, Washington 98124

ABSTRACT

The report investigates scattering from a rough surface when transmitter and receiver are at a finite distance from each other, so that the sphericity of the incident and scattered waves has to be taken into account. The calculation is complicated by the fact that, unlike the case of plane waves, the equiprobability planes of the surface do not coincide with the equiphase surfaces, and therefore a number of simplifying assumptions are made, in particular, geometric optics are used. The phase distribution of the scattered field by approximate integrations. From this, the other quantities of interest can be found. The results are compared with the measurements performed by Beard using microwaves and a random water surface with known statistical properties.

TABLE OF CONTENTS

	Page
LIST OF FIGURES	i
1. INTRODUCTION	1
2. PHASE DISTRIBUTION OF THE SCATTERED FIELD	4
3. ROTATION OF THE VARIANCE ELLIPSE	10
4. CALCULATION OF THE PHASE QUADRATURE COMPONENTS OF THE SCATTERED FIELD	14
5. MODIFICATION FOR SURFACES GENERATED BY A NARROW-BAND PROCESS	19
6. COMPARISON WITH EXPERIMENTAL DATA	22
7. CONCLUSION	30
APPENDIX	32
REFERENCES	34

LIST OF FIGURES

	<u>Page</u>
Fig. 1. Equiprobability and equiphase surfaces.	3
Fig. 2. Qualitative derivation of the phase distribution.	3
Fig. 3. Asymmetrical character of the phase distribution.	5
Fig. 4. Basic quantities for calculating the phase distribution.	5
Fig. 5. The variance ellipse for the scattered field.	11
Fig. 6. Single saddle point used for a wide-band process.	21
Fig. 7. Several saddle points contribute to the integration for a narrow-band process; this is equivalent to using a single saddle point of the slowly varying envelope of the process and its correlation function.	21
Fig. 8. Rotation of the variance ellipse. Experimental data by Beard (1965), theoretical curve computed by (57).	25
Fig. 9. RMS scattered amplitude. Experimental data by Beard (1967), theoretical curve computed by (62).	27
Fig. 10. Extreme values of the variance of the scattered field. Experimental data by Beard (1965), theoretical curve computed by (87).	28
Fig. 11. Ratio of extreme variances of the scattered field. Experimental data by Beard (1967), theoretical curve computed by (66). For the reason of the discrepancy, see last paragraph of Section 4, p. 19.	29

1. INTRODUCTION

When a rough surface generated by a stationary random process is illuminated by a plane wave and the scattered field is observed far in the Fraunhofer zone (i.e., the scattered waves may be considered plane), the reflection points on the surface resulting in the same phase ϕ at the receiving point are on a plane $z = \text{const}$, where z is measured from the mean plane of the surface. These equiphase planes are thus identical with the equiprobability planes $Z = z$, where Z is the deviation of the surface from its mean plane, a random variable (here assumed normal).

The ultimate root of the difficulties encountered in an investigation of non-plane wave illumination and scattering is the fact that the equiphase surfaces are no longer identical with the equiprobability surfaces. The equiprobability surfaces are given by $p(z) = \text{const}$, where $p(z)$ is the probability density of Z ; as before, the equiprobability surfaces are therefore given by the planes $z = \text{const}$ (Figure 1). However, the locus of reflection points yielding the same phase at the receiver, when both are at a height h above $\langle Z \rangle$ and separated by a distance D , is a rotational ellipsoid with foci at the transmitting and receiving points, T_x and R_x , respectively.

The resulting phase distribution at the receiver will under these conditions be asymmetrical, which leads to further consequences rarely met in plane wave propagation. To see qualitatively why the phase distribution is asymmetrical, consider the case when the standard deviation σ_w of the surface is very small so that the surface deviates only very slightly from a plane (Figure 2). For plane wave illumination and scattering, this would obviously result in a received phase that only very slightly deviates from its mean. However, for spherical waves, the phase is given by $\phi = k(r_1 + r_2)$. Let the point $x = 0, y = 0$ (when $Z = 0$) give rise to a phase ϕ_0 . Smaller phases are possible, though not very probable; they will occur only when $Z(0,0)$ goes positive. On the other hand, phases larger than ϕ_0 will occur very often, since practically any reflecting point with coordinates other than $x = 0, y = 0$ will give rise to a phase larger than ϕ_0 . The phases near the value ϕ_0 will

occur for reflecting points in the first Fresnel zone, and since this is the largest, the probability density of ϕ can be expected to have a maximum near this value. For the reasons just given, this probability density should then fall off quickly from this maximum towards smaller ϕ , and slowly towards larger ϕ as shown in Figure 3. Thus, $p(\phi)$ will be asymmetrical.

The main effort of this report is to derive this phase distribution; once this is established, the other quantities of interest, in particular, the distribution of the scattered field, and hence the mean scattered power, the behavior of the phase-quadrature components, etc., can be derived from this phase distribution by previously established methods (Beckmann, 1962; Beckmann and Spizzichino, 1963).

The calculation is involved and it was not found possible to arrive at practically useful results unless a number of simplifying assumptions were made. These are the following:

- (A) Geometric optics are valid; only waves reflected from a favorable, or nearly favorable, slope (making the local angle of incidence equal to the local angle of reflection) will reach the receiver.
- (B) The equiphase surfaces are elliptical cylinders rather than rotational ellipsoids; near the plane $y = 0$ (where most reflections must be expected) the two are identical and thus the problem is reduced from a 3-dimensional one to a 2-dimensional one.
- (C) The transmitting and receiving antennas are at the same height h above the mean rough surface.
- (D) The rough surface is generated by a stationary normal process in the x direction.

Assumptions (C) and (D) may be withdrawn at the cost of mathematical simplicity, and the same is essentially true of Assumption (B), though this will lead to integrals of almost prohibitive complexity; but Assumption (A) is essential to the method to be used.

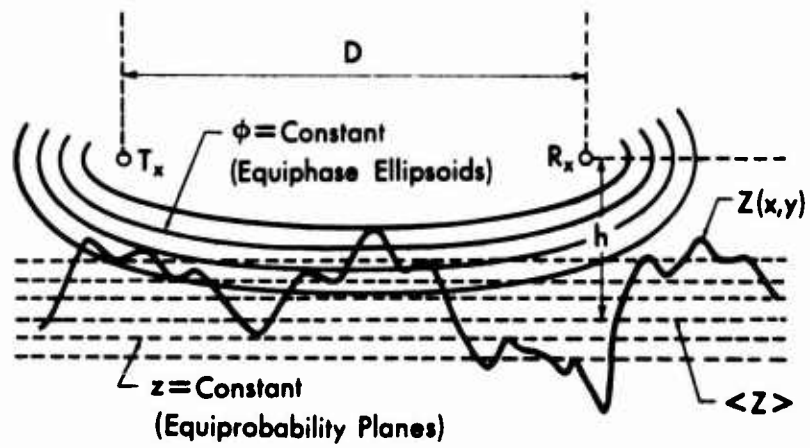


Fig. 1. Equiprobability and equiphase surfaces.

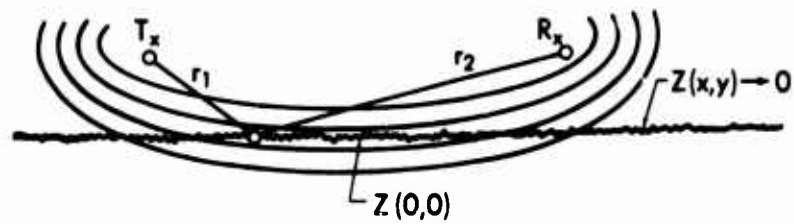


Fig. 2. Qualitative derivation of the phase distribution.

In addition to the above simplifying assumptions, approximate procedures are used to evaluate some otherwise intractable integrals. In spite of this coarse treatment, the final results appear to be at least in qualitative agreement with experimental results, so that the method should be useful for providing physical insight, if not precise numerical results.

2. PHASE DISTRIBUTION OF THE SCATTERED FIELD

Consider the distance (or "geometric phase") ϕ from T_x to R_x via a reflection point P (Figure 4).^{*} For a given ϕ , the reflection point must lie on an ellipse with semimajor axis

$$a = \frac{1}{2}\phi \quad (1)$$

and semiminor axis

$$b = \frac{\sqrt{\phi^2 - D^2}}{2} \quad (2)$$

where $D = 2d$ is the distance between transmitter and receiver. The equation of the ellipse is

$$\frac{z^2}{b^2} + \frac{x^2}{a^2} = 1 \quad (3)$$

In the following only the lower left quadrant of the ellipse is considered: the upper quadrants are irrelevant because the surface $Z(x)$ has such a small standard deviation σ_w that it is practically impossible for $Z(x) \geq h$ to be satisfied, and the lower right quadrant only reinforces all effects by symmetry.

Consider now a fixed propagation distance or geometric phase ϕ assuming that the reflection point was located near a height $Z = z$. This uniquely determines the x coordinate of the reflection point and is determined from (3) for $Z = z$:

$$x_z = - \frac{a\sqrt{b^2 - z^2}}{b} \quad (4)$$

^{*}Upper and lower case ϕ and ϕ , respectively the geometric and electrical phases, are sufficiently similar in form that care should be exercised to prevent confusion.

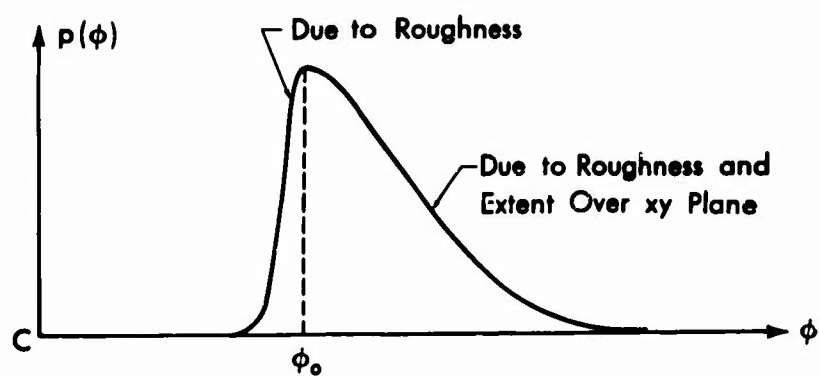


Fig. 3. Asymmetrical character of the phase distribution.

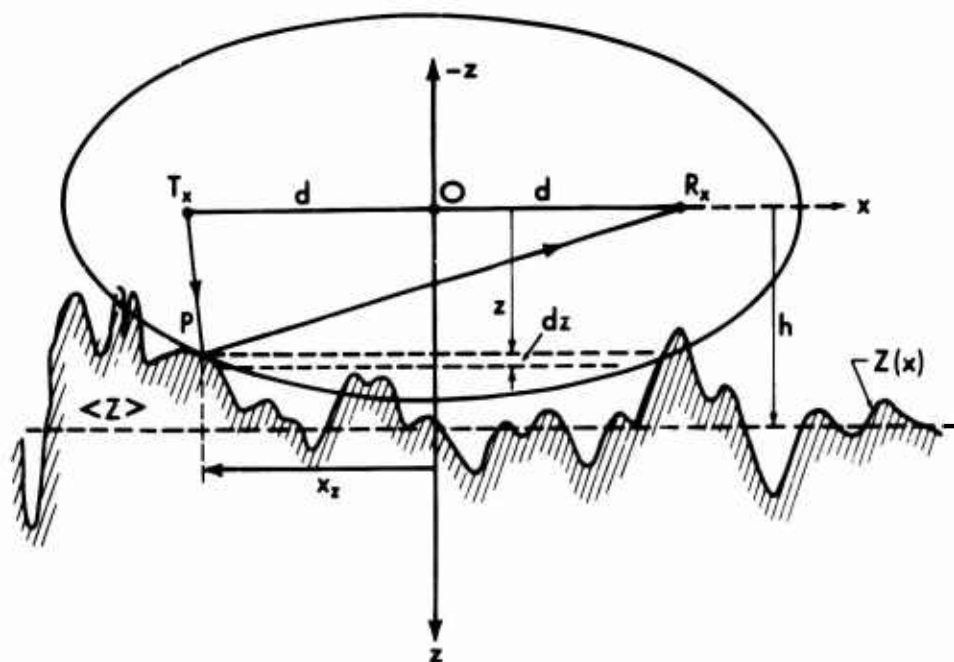


Fig. 4. Basic quantities for calculating the phase distribution.

The slope of the ellipse at any point is from (3)

$$Z'(x) = \frac{bx}{a\sqrt{a^2 - x^2}} \quad (5)$$

and hence the slope at the reflection point (if reflection towards the receiver is to occur) must be, as obtained by substituting (4) for x ,

$$Z'(x_z) = \frac{b\sqrt{b^2 - z^2}}{a_z} \quad (6)$$

The probability of this being the case is found from the distribution of Z' , which is normal and stationary, since Z is normal and stationary, with mean square value

$$\sigma'^2 = \langle Z'^2 \rangle = -B''(0) \quad (7)$$

where $B(\tau)$ is the correlation function of $Z(x)$.

Thus, the density of Z' is

$$p(z') = \frac{\tau}{\sigma_w \sqrt{2\pi}} \exp\left(-\frac{\tau^2 z'^2}{2\sigma_w^2}\right) \quad (8)$$

where

$$\tau = \frac{\sigma_w}{\sigma'} \quad (9)$$

This quantity, which has the dimension of a length, is in effect a decorrelation distance; if the correlation function is Gaussian, τ is equal to the correlation distance defined as the distance for which the autocorrelation coefficient decreases to e^{-1} ; for other correlation functions, τ differs from the correlation distance only by a constant factor. Note that σ' is the rms slope of the surface.

From (6), (7) and (8) we obtain the conditional probability density of ϕ given that the reflection takes place at height z :

$$p(\phi|z) = \frac{\tau}{\sigma_w \sqrt{2\pi}} \exp \left[-\frac{b^2(b^2 - z^2)\tau^2}{2a^2 z^2 \sigma_w^2} \right] \quad (10)$$

where ϕ is contained implicitly in the quantities a and b through (1) and (2).

The probability distribution $p(\phi)$ is now obtained from the Theorem of Total Probability by integrating over all z :

$$p(\phi) = \int_{-\infty}^{\infty} p(\phi|z)p(z)dz \quad (11)$$

where the density of z is

$$p(z) = \frac{1}{\sigma \sqrt{2\pi}} \exp \left[-\frac{(z - h)^2}{2\sigma_w^2} \right] \quad (12)$$

Substituting (10) and (12) in (11) we obtain

$$p(\phi) = \frac{\tau}{2\pi\sigma_w^2} \int_{-\infty}^{\infty} \exp \left[-\frac{b^2\tau^2(b^2 - z^2)}{2a^2 z^2 \sigma_w^2} - \frac{(z - h)^2}{2\sigma_w^2} \right] dz \quad (13)$$

To evaluate this integral exactly is a fairly hopeless task, and therefore the Laplace method of integration is used. We denote the exponent by $E(z)$ and find the point z_0 for which it is maximum from the condition

$$E'(z) = 0 \quad (14)$$

Expanding the exponent in the neighborhood of this point (from which the integral obtains its greatest contribution), we obtain on retaining terms up to the quadratic term,

$$\begin{aligned} p(\phi) &= \frac{\tau e^{E(z_0)}}{2\pi\sigma_w^2} \int_{-\infty}^{\infty} \exp \left[\frac{E''(z_0)}{2} (z - z_0)^2 \right] dz \\ &= \frac{e^{E(z_0)}}{\sqrt{2\pi} \sigma_w^2 \sqrt{-E''(z_0)}} \end{aligned} \quad (15)$$

To solve the cubic equation resulting from (14), we obtain by Newton's method

$$z_0 \approx h \quad (16)$$

so that after some algebra one obtains

$$p(\phi) = \frac{\tau \exp\left[-\frac{b^2 \tau^2 (b^2 - h^2)}{2a^2 h^2 \sigma_w^2}\right]}{s(\phi)} \quad (17)$$

where

$$s(\phi) = \sigma_w \sqrt{2\pi \left(1 + \frac{3b^4 \tau^2}{a^2 h^4}\right)} \quad (18)$$

Substituting from (1) and (2), this yields

$$p(\phi) = \frac{\tau}{\sigma_w s(\phi)} \exp\left[-\frac{(\phi^2 - D^2)(\phi^2 - D^2 - 4h^2)\tau^2}{8\phi^2 h^2 \sigma_w^2}\right] \quad (19)$$

Note that this expression has been obtained from (13) by considering the contribution from the region near $z = h$, but that the result will be accurate only if the factor multiplying $(z - z_0)^2$ is large (guaranteeing that almost all of the contribution to the integral is concentrated into the considered region), i.e.,

$$\frac{b^2 \tau^2}{2a^2 \sigma_w^2} \gg 1 \quad (20)$$

In practical applications $\sigma_w \ll \tau$, so that (20) will be well satisfied for probable phases ϕ , for which a is of the same order as b . However, for the highly improbable phases $\phi \rightarrow D$ (corresponding to the surface rising to a height where it will interrupt the direct ray from transmitter to receiver), the ellipse will approach the segment $T_x R_x$, $b \rightarrow 0$, and (20) is violated. Thus (19) is valid only for probable

phases or larger. To restore the validity of (19) we therefore only need to impose a lower limit on ϕ . This is found as follows. We consider the normal distribution of the surface truncated at $h - 3\sigma_w$ (incurring an error of less than 0.5 percent), which corresponds to a minimum phase (attained only at the point $x = 0$)

$$\phi_m = \sqrt{D^2 + 4(h - 3\sigma_w)^2} \quad (21)$$

or, since by assumption $\sigma_w \ll h$,

$$\phi_m = \sqrt{D^2 + 4h^2} \quad (22)$$

The phase distribution may then be written in the form

$$p(\phi) = \frac{C\tau}{\sigma_w s(\phi)} \exp - \left[\frac{(\phi^2 - D^2)(\phi^2 - \phi_m^2)\tau^2}{8\phi^2 h^2 \sigma_w^2} \right] \quad (23)$$

where the normalization constant C is found from the condition that (23) must integrate to unity. To perform this integration, the Laplace method of integration is again used. The exponent is now maximum for

$$\phi_o = \sqrt{\phi_m D} \quad (24)$$

But, since from (22)

$$\phi_m = D \left(1 + \frac{h^2}{2D^2} \right) \quad (25)$$

and in practical applications $h/D \ll 1$, we are justified in writing (24) as

$$\phi_o \approx \phi_m \quad (26)$$

Substituting for $s(\phi)$ from (18) and noting that

$$h^4(\phi_m) = \frac{(\phi_m^2 - D^2)^2}{16} = h^4 \quad (27)$$

we find

$$s(\phi_m) = \sqrt{2\pi \left(1 + \frac{3\pi^2}{D^2 + 4h^2}\right)} \approx \sqrt{2\pi} \quad (28)$$

so that the phase distribution is from (23)

$$p(\phi) = \frac{\tau}{h\sigma_w} \sqrt{\frac{2}{\pi}} \exp \left[-\frac{\tau^2(\phi^2 - \phi_m)^2(\phi^2 - D^2)}{8\phi^2 h^2 \sigma_w^2} - h^2/2D^2 \right] \quad (29)$$

or, if it is approximated by its expansion near its maximum as above,

$$p(\phi) = \frac{\tau}{h\sigma_w} \sqrt{\frac{2}{\pi}} \exp \left[-\frac{\tau^2(\phi - \phi_m)^2}{2h^2 \sigma_w^2} \right] \quad (\phi_m \leq \phi \leq \infty) \quad (30)$$

Transforming from the geometric phase ϕ to the electrical phase ϕ through

$$\phi = k\phi = \frac{2\pi}{\lambda} \phi \quad (31)$$

we finally find

$$p(\phi) = \frac{\tau}{kh\sigma_w} \sqrt{\frac{2}{\pi}} \exp \left[-\frac{(\phi - \phi_m)^2 \tau^2}{2k^2 h^2 \sigma_w^2} \right] \quad (\phi_m \leq \phi \leq \infty) \quad (32)$$

where

$$\phi_m = k\phi_m = k\sqrt{D^2 + 4h^2} \quad (33)$$

This is the phase distribution to be used for the calculation of the scattered field.

3. ROTATION OF THE VARIANCE ELLIPSE

The phase of the received field is a random variable, and the received field is therefore conveniently decomposed into two components;

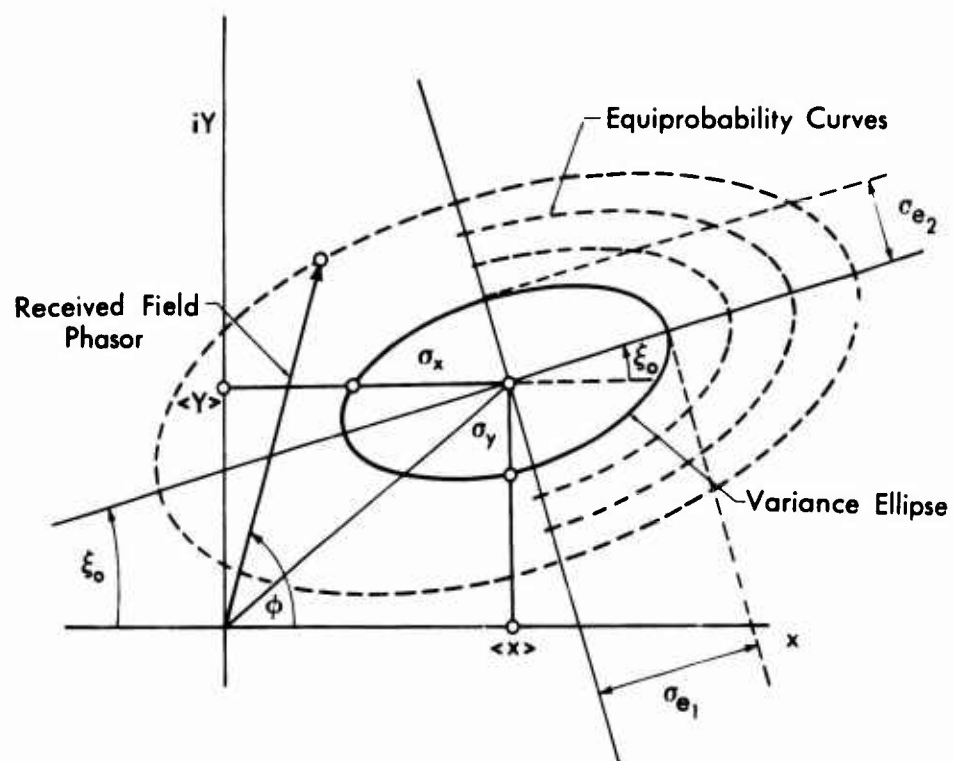


Fig. 5. The variance ellipse for the scattered field.

one in phase with the field reflected by a smooth plane, and the other perpendicular to it. These two components will be referred to as the real and imaginary component, respectively, of the scattered field, since it is convenient to plot the received field in the complex plane. Since both components represent the sum of a large number of random quantities, namely the waves scattered from each of the reflection points on the surface, both components will be normal and the received field is therefore described by a two-dimensional normal distribution (real component X , imaginary component Y). The equiprobability curves for the two-dimensional normal distribution, as is easily shown by analytical geometry, are ellipses centered at $X = \langle X \rangle$, $Y = \langle Y \rangle$; their axes have identical directions, one of which makes an angle ξ_0 with the real axis X (the other direction differs by 90°). The angle ξ_0 is found from the relation

$$\tan 2\xi_0 = \frac{2\text{cov}(X,Y)}{\sigma_X^2 - \sigma_Y^2} \quad (34)$$

where σ_X^2 , σ_Y^2 are the variances of the X and Y components, respectively. Thus, the ellipses of the family of equiprobability curves differ only by their major and minor axes; the centers and directions are identical. One of these is the "variance ellipse"; this is the one whose major and minor axes σ_{e1} , σ_{e2} (not necessarily respectively), are related to the variances of X and Y through

$$\sigma_{e1}^2 + \sigma_{e2}^2 = \sigma_X^2 + \sigma_Y^2 \quad (35)$$

It can be shown that

$$\left. \begin{aligned} \sigma_X^2 &= \sigma_{e1}^2 \cos^2 \xi_0 + \sigma_{e2}^2 \sin^2 \xi_0 \\ \sigma_Y^2 &= \sigma_{e1}^2 \sin^2 \xi_0 + \sigma_{e2}^2 \cos^2 \xi_0 \end{aligned} \right\} \quad (36)$$

and hence

$$\left. \begin{aligned} \sigma_{e1}^2 &= \frac{\sigma_X^2 \cos^2 \xi_o - \sigma_Y^2 \sin^2 \xi_o}{\cos 2\xi_o} \\ \sigma_{e2}^2 &= \frac{\sigma_Y^2 \cos^2 \xi_o - \sigma_X^2 \sin^2 \xi_o}{\cos 2\xi_o} \end{aligned} \right\} \quad (37)$$

To relate these quantities to the phase distribution $p(\phi)$, we note that in our geometric-optics model the received field is produced by the interference of the waves reflected by n reflection points on the surface, so that (apart from an unknown constant of proportionality which can be absorbed into the equally unknown number n)

$$X = \sum_{j=1}^n \cos \phi_j \quad Y = \sum_{j=1}^n \sin \phi_j \quad (38)$$

Denoting the means of X and Y by

$$\alpha = n \int p(\phi) \cos \phi d\phi \quad (39)$$

$$\beta = n \int p(\phi) \sin \phi d\phi \quad (40)$$

we find the variances in the form

$$\sigma_X^2 = \frac{n}{2} \left[1 + \int p(\phi) \cos 2\phi d\phi - \frac{2\alpha^2}{n^2} \right] \quad (41)$$

$$\sigma_Y^2 = \frac{n}{2} \left[1 - \int p(\phi) \cos 2\phi d\phi - \frac{2\beta^2}{n^2} \right] \quad (42)$$

The covariance of X and Y is after a little manipulation using the fact that the ϕ_j are independent found to be

$$\text{cov}(X, Y) = n \int p(\phi) \cos \phi \sin \phi d\phi - \frac{\alpha\beta}{n} \quad (43)$$

so that on substituting the last three results in (34) we obtain

$$\tan 2\xi_0 = \frac{\int p(\phi) \sin 2\phi d\phi - \frac{2\alpha\beta/n^2}{\int p(\phi) \cos 2\phi d\phi - \frac{\alpha^2 - \beta^2}{n^2}} \quad (44)$$

This relation reveals a marked difference between the scattering of plane and spherical waves from a normal (or any other symmetrically distributed) surface: For plane waves, the phase distribution of a symmetrically distributed surface is also symmetrical, so that the denominator of (44) vanishes (or, if other coordinates are introduced, is constant); for spherical waves emanating from the transmitter at a finite distance from the surface, however, we found a symmetrically (normally) distributed surface to result in an asymmetrical phase distribution (32), so that as the variance of the surface, and hence the variance of ϕ increases, ξ_0 will by (44) change, i.e., the variance ellipse will rotate.

Relations (39) through (44) establish the connection between the scattered field and the phase distribution. In the next section, these quantities will be evaluated when (32) is substituted for $p(\phi)$.

4. CALCULATION OF THE PHASE QUADRATURE COMPONENTS OF THE SCATTERED FIELD

To find the mean of the real component of the scattered field, we substitute (32) in (39); on setting $\phi - \phi_m = t$, this becomes

$$\alpha = \frac{n\tau}{kh\sigma_w} \sqrt{\frac{2}{\pi}} \int_0^\infty \exp\left[-\frac{t^2 t^2}{2k^2 h^2 \sigma_w^2}\right] \cos(t + \phi_m) dt \quad (45)$$

On expanding the cosine, the two resulting integrals can be evaluated by using the integrals

$$\int_0^\infty e^{-At^2} \cos Bt dt = \frac{1}{2} \sqrt{\frac{\pi}{A}} e^{-B^2/4A} \quad (46)$$

and

$$\int_0^\infty e^{-At^2} \sin Bt dt = \frac{B}{2A} e^{-B^2/4A} {}_1F_1\left(\frac{1}{2}; \frac{3}{2}; B^2/4A\right) \quad (47)$$

where ${}_1F_1$ is the confluent hypergeometric function. After some tedious, though straightforward, calculations, the result can be expressed in terms of the parameter

$$\kappa = \frac{k^2 h^2 \sigma_w^2}{2\tau^2} \quad (48)$$

and the auxiliary variables

$$\xi = e^{-\kappa}, \quad \eta = \sqrt{\frac{\kappa}{\pi}} e^{-\kappa} {}_1F_1\left(\frac{1}{2}; \frac{3}{2}; \kappa\right) \quad (49)$$

Then (45) yields

$$\alpha = n(\xi \cos \phi_m - \eta \sin \phi_m) \quad (50)$$

Similarly, for the mean of the imaginary component one finds

$$\beta = n(\xi \sin \phi_m + \eta \cos \phi_m) \quad (51)$$

To evaluate the integrals occurring in (44), we introduce the auxiliary quantities

$$\mu = e^{-4\kappa}, \quad \nu = 2\sqrt{\frac{\kappa}{\pi}} e^{-4\kappa} {}_1F_1\left(\frac{1}{2}; \frac{3}{2}; 4\kappa\right) \quad (52)$$

One then finds

$$\int_{\phi_m}^{\infty} p(\phi) \cos 2\phi d\phi = \mu \cos 2\phi_m - \nu \sin 2\phi_m \quad (53)$$

$$\int_{\phi_m}^{\infty} p(\phi) \sin 2\phi d\phi = \mu \sin 2\phi_m + \nu \cos 2\phi_m \quad (54)$$

so that on substituting these results in (44) one obtains

$$\tan 2\xi_o = \frac{\tan 2\phi_m + \frac{\nu - 2\xi\eta}{\mu - \xi^2 + \eta^2}}{1 - \frac{\nu - 2\xi\eta}{\mu - \xi^2 + \eta^2} \tan 2\phi_m} \quad (55)$$

This can be written in the form

$$\xi_o = \phi_m + \frac{1}{2} \arctan \frac{\nu - 2\xi\eta}{\mu - \xi^2 + \eta^2} \quad (56)$$

or discarding the auxiliary variables by (49) and (52),

$$\xi_o = \phi_m + \frac{1}{2} \arctan \left[2 \sqrt{\frac{\kappa}{\pi}} \frac{e^{-2\kappa} {}_1F_1\left(\frac{1}{2}; \frac{3}{2}; 4\kappa\right) - {}_1F_1\left(\frac{1}{2}; \frac{3}{2}; \kappa\right)}{\frac{\kappa}{\pi} {}_1F_1^2\left(\frac{1}{2}; \frac{3}{2}; \kappa\right) - 1 + e^{-2\kappa}} \right] \quad (57)$$

Since by (48) κ is proportional to σ_w^2 , this establishes the rotation of the variance ellipse with the variance σ_w^2 of the rough surface.

For practical applications, the approximate expressions of ${}_1F_1$ for small and large κ are listed here for reference purposes:

$${}_1F_1\left(\frac{1}{2}; \frac{3}{2}; \kappa\right) = 1 + \frac{1}{3} \kappa \quad (\kappa \ll 1) \quad (58)$$

$${}_1F_1\left(\frac{1}{2}; \frac{3}{2}; \kappa\right) \sim \frac{e^\kappa}{2\kappa} \quad (\kappa \gg 1) \quad (59)$$

For the variances of the real and imaginary components one obtains from (41), (42), and (53), (54)

$$\sigma_X^2 = \frac{n}{2} \left[1 + \mu \cos 2\phi_m - \nu \sin 2\phi_m - 2(\xi \cos \phi_m - \eta \sin \phi_m)^2 \right] \quad (60)$$

$$\sigma_Y^2 = \frac{n}{2} \left[1 - \mu \cos 2\phi_m + \nu \sin 2\phi_m - 2(\xi \sin \phi_m + \eta \cos \phi_m)^2 \right] \quad (61)$$

The total variance of the scattered field, which is proportional to the incoherently scattered power (at the receiving point) is therefore

$$\sigma^2 = \sigma_x^2 + \sigma_y^2 = n(1 - \xi^2 - \eta^2) \quad (62)$$

As was to be expected, this is independent of ϕ_m . The above relation also satisfies the physical requirements

$$\lim_{\sigma_w \rightarrow 0} \sigma^2 = \lim_{\kappa \rightarrow 0} \sigma^2 = 0 \quad (63)$$

$$\lim_{\sigma_w \rightarrow \infty} \sigma^2 = \lim_{\kappa \rightarrow \infty} \sigma^2 = n \quad (64)$$

To find the ratio of the major to the minor axis of the variance ellipse

$$K = \frac{\sigma_{\max}}{\sigma_{\min}} = \left(\frac{\sigma_{e1}}{\sigma_{e2}} \right)^{\pm 1} \quad (65)$$

where the exponent +1 or -1 is chosen so as to make $K^2 \geq 1$, we take the ratio of the two expressions in (37), obtaining

$$K^2 = \left(\frac{k^2 - \tan^2 \xi_o}{1 - k^2 \tan^2 \xi_o} \right)^{\pm 1} \quad (66)$$

where

$$k^2 = \frac{\sigma_x^2}{\sigma_y^2} \quad (67)$$

or substituting from (60) and (61),

$$k = \frac{1 - \xi^2 - \eta^2 + (\eta^2 - \xi^2 + \mu) \cos 2\phi_m + (2\xi\eta - \nu) \sin 2\phi_m}{1 - \xi^2 - \eta^2 - (\eta^2 - \xi^2 + \mu) \cos 2\phi_m - (2\xi\eta - \nu) \sin 2\phi_m} \quad (68)$$

so that k^2 , and hence K^2 , depend on ϕ_m , i.e., on the geometric configuration determined (with accuracy of a fraction of a wavelength) by D and h in (33). For $\sigma_w \rightarrow \infty$, i.e., $\kappa \rightarrow \infty$, (67) yields $k \rightarrow 1$, hence

$$\lim_{\sigma_w \rightarrow \infty} K^2 = 1 \quad (69)$$

The limit $\sigma_w \rightarrow 0$, i.e., $\kappa \rightarrow 0$, is more difficult to establish, since

$$\left. \begin{aligned} \lim_{\kappa \rightarrow 0} \xi &= \lim_{\kappa \rightarrow 0} \mu = 1 \\ \lim_{\kappa \rightarrow 0} \eta &= \lim_{\kappa \rightarrow 0} \nu = 0 \end{aligned} \right\} \quad (70)$$

so that for $\kappa \rightarrow 0$, (68) becomes an indeterminate expression of type $0/0$. Expanding ξ , η , μ and ν in terms of κ , we find

$$k^2 = \frac{\kappa \left(2 - \frac{1}{\pi}\right) - \kappa \left(2 - \frac{1}{\pi}\right) \cos 2\phi_m - 2\kappa \sqrt{\frac{\kappa}{\pi}} \sin 2\phi_m + \dots}{\kappa \left(2 - \frac{1}{\pi}\right) + \kappa \left(2 - \frac{1}{\pi}\right) \cos 2\phi_m + 2\kappa \sqrt{\frac{\kappa}{\pi}} \sin 2\phi_m + \dots} \quad (71)$$

so that

$$\lim_{\kappa \rightarrow 0} k^2 = \frac{1 - \cos 2\phi_m}{1 + \cos 2\phi_m} = \tan^2 \phi_m \quad (72)$$

After a similar procedure one obtains from (56)

$$\lim_{\kappa \rightarrow 0} \xi_0 = \phi_m \pm \frac{m\pi}{2} \quad (m = 0, 1) \quad (73)$$

Substituting (72) and (73) in (66), we have

$$\lim_{\sigma_w \rightarrow 0} K^2 = \infty \quad (74)$$

It will later be found that (69) agrees with experiment, but (74) does not. The reason is that (69) can be derived directly from (41), (42) and (67) for any distribution $p(\phi)$; on the other hand, the above derivation shows that (74) depends very critically on the distribution $p(\phi)$, for a minute change in the latter will lead to a completely different limit (74). For example, if $\phi_m = m\pi$ ($m = 1, 2, \dots$), then the indeterminate expression $0/0$ in (68) cannot be resolved until the quadratic terms (i.e., terms in σ_w^4) are taken into account. Obviously, the approximations used in deriving $p(\phi)$ cannot achieve the required accuracy of up to and including fourth-order terms in σ_w .

This point is noted here because (74) is the one result that does not agree qualitatively with experimental observations.

5. MODIFICATION FOR SURFACES GENERATED BY A NARROW-BAND PROCESS

The underlying idea of a saddle-point integration in physical optics to calculate the scattered field is the summation of the contributions to the scattered wave from the neighborhood of a point with favorable slope on the surface. (Saddle-point methods in physical optics thus represent a transition to geometric optics.) As the distance from that point increases, the slope will change to a less favorable one, which means that the scattered wavelets will increasingly be out of phase with the one scattered from the favorable slope, and therefore both the scattered wave and the integral will cease to obtain contributions as the immediate neighborhood of a favorable slope is abandoned. This is schematically shown in Figure 6 for a wide-band random process.

However, for a narrow-band process the situation is somewhat different. A (mean-square continuous) narrow-band process consists of random oscillations modulated by a slowly varying random envelope (Beckmann, 1967, pp. 249-254). As shown in Figure 7, several successive oscillations will produce a succession of points of the type in Figure 6 reflecting favorable phases.

In calculating the field by physical optics, the entire correlation function (which itself also consists of oscillations modulated by a slowly varying envelope) is required, but this problem will take care of itself, since there will be a corresponding succession of saddle points whose contributions will add up to yield the total scattered field. However, since the above analysis utilizes not the entire correlation function (as it would in physical optics), but only the RMS slope in (9), the slope needed is not the slope of the random process itself, but that of its envelope. The reason is that in geometric optics one looks for the slopes that will concentrate waves with equal phases; it is obvious from Figure 7 that this will be the slope of the envelope of a narrow-band process, and not the slope of the narrow-band process itself (which is much larger). It can be shown [Beckmann, 1967, pp. 250-253, (7-3.8), (7.3-26), (7.3-30)] that the correlation function of this envelope is equal to the envelope of the correlation function

$$B(\tau) = a(\tau) \cos \omega_0 \tau \quad (75)$$

of a narrow-band process whose spectrum is symmetrical about some frequency ω_0 ; its rms slope is therefore

$$\sigma_{\text{env}}^1 = \sqrt{-a''(0)} = \frac{\sigma_w}{\tau_{\text{env}}} \quad (76)$$

so that

$$\tau_{\text{env}} = \frac{\sigma_w}{\sqrt{-a''(0)}} \quad (77)$$

Since from (75)

$$a''(0) = B''(0) + \sigma_w^2 \omega_0^2 \quad (78)$$

and $B''(0) < 0$, we have

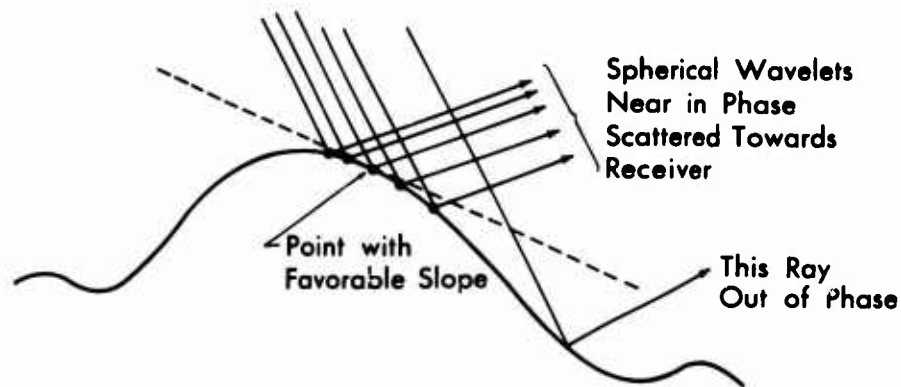


Fig. 6. Single saddle point used for a wide-band process.

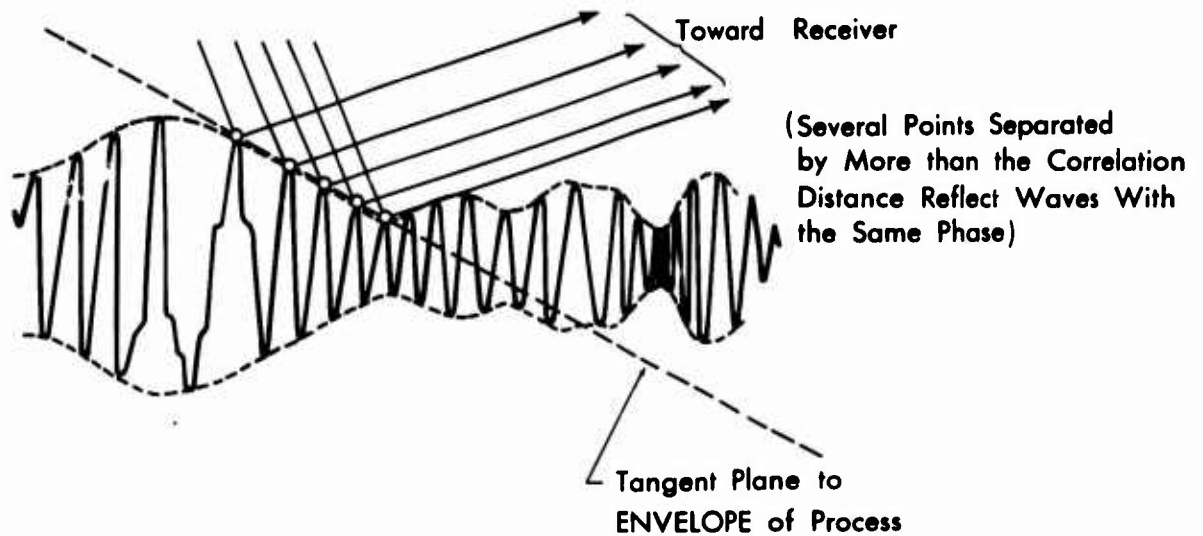


Fig. 7. Several saddle points contribute to the integration for a narrow-band process; this is equivalent to using a single saddle point of the slowly varying envelope of the process and its correlation function.

$$\tau_{\text{env}} = \frac{\sigma_w}{\sqrt{|B''(0)| - \sigma_w^2 \omega_0^2}} = \frac{1}{\sqrt{|\rho''(0)| - \omega_0^2}} \quad (79)$$

where

$$\rho(\tau) = \frac{B(\tau)}{\sigma_w^2} \quad (80)$$

is the autocorrelation coefficient of the random surface.

6. COMPARISON WITH EXPERIMENTAL DATA

There have apparently been only two detailed experiments performed to investigate scattering from a rough surface at a finite distance from transmitter and receiver, one by Beard (1965, 1967), and the other by Clarke and Hendry (1964). Of these, however, only Beard has measured the parameters determined directly by the phase, namely ξ_0 , σ_{e1} , σ_{e2} ; Clarke and Hendry have only measured the equivalent of σ_x , σ_y , which is ambiguous for determining the variance ellipse, as can be seen from Figure 5, for ξ_0 will change with σ_w as shown by (44), (57), and as also follows from Beard's experiments.

Beard (1965, 1967) illuminated a rough water surface by microwaves with wavelength $\lambda = 2.83$ cm. The surface of water in a tank was perturbed by injecting air or water into the water tank (in a region beyond the illuminated area). By varying the injection rate, the standard deviation σ_w of the water surface could be varied. The transmitter and receiver antennas were separated by a distance $D = 4.115$ m (162 inches); both were situated at a height $h = 0.869$ m above the mean water level, yielding a grazing angle $\psi = 22.9^\circ$ at the origin $Z(0,0)$ in Figure 2.

The distribution of the deviation of the water surface Z was measured by Beard (1965) and found normal. The correlation function of the surface was measured by Beard in 1966; these data, partly not yet published, were at the author's disposal to enable the above theory to be compared with experiment. These measurements show that the random

process generating the water surface is narrow-band with a central frequency $\frac{\omega}{2\pi} = 2.37$ c/s. The water waves thus generated propagate with a velocity (Stoker, 1957)

$$v = \frac{G}{\omega} = 0.6584 \text{ m/s} \quad (81)$$

where $G = 9.81 \text{ m/s}^2$ is the gravitational acceleration. Beard's measurements (1967) show that the water surface can be considered partially "frozen" and moving along the water tank with the group velocity, which is one-half of the phase velocity (81) for deep water waves. It was also established that the surface is strongly anisotropic; i.e., the correlation distance in the direction perpendicular to the waterflow (y) is much larger than in the direction along the water flow (x), so that the assumption of one-dimensional roughness is to some extent justified (assumption D, p. 2, assumes an infinite correlation distance in the y direction).

The correlation function envelope corresponding to a (τ) in (75) was found to be very close to an exponential curve for larger τ [see Figure 8 in (Beard, 1966)]; however, for $\tau \rightarrow 0$, it has so far not been possible to accurately measure $B(\tau)$ and its derivatives; i.e., direct measurement of the mean square slope and the correlation distance defined through it by (9), has not yet been performed. On the other hand, indirect inference of τ_{env} from the measured data, i.e., by (70), is not very accurate, since $B''(\tau)$ is not known for $\tau \rightarrow 0$. By use of various methods of estimating τ_{env} from the measured data, it was found that τ_{env} is of the order of 1 meter.

Beard's experimental results (1965, 1967) are plotted as a function of the variable

$$\frac{\sigma_w \sin \psi}{\lambda} = g \quad (82)$$

The variable κ used in the above analysis and defined by (48) is therefore related to g by

$$\sqrt{\kappa} = \frac{D\pi}{\tau_{\text{env}} \sqrt{2} \cos \psi} g \quad (83)$$

For the values $D = 4.115$ m and $\psi = 22.9^\circ$ used in the experiment, this makes

$$\sqrt{\kappa} = \frac{9.89}{\tau_{\text{env}}} g \quad (84)$$

As τ_{env} is of the order of 1 m, but its exact value is not known, the value $\tau_{\text{env}} = 0.989$ m was assumed so that (84) reduces to the numerically convenient relation

$$\sqrt{\kappa} = 10 g \quad (85)$$

In Beard's experiment (1965), the random amplitudes of two components of the scattered field in phase quadrature were investigated. The phase of these components with respect to the coherent part of the field could be varied at will [which was not the case in the experiment by Clarke and Hendry (1964)], so that all characteristics of the variance ellipse in Figure 5, namely ξ_0 , σ_x , σ_y , σ_{e1} , σ_{e2} and $K^2 = \sigma_{\text{max}}^2 / \sigma_{\text{min}}^2$ could be directly measured.

The data measured by Beard for ξ_0 as a function of σ_w in one of the experiments (Beard, 1965, Figure 29) are shown in Figure 8. This is compared with the theoretically derived formula (57) where κ , given by (48), is converted to g through (85). Equation (57) also contains the additive constant ϕ_m given by (33). This constant cannot be accurately determined, since ϕ_m is of the order of hundreds of wavelengths, and ϕ_m is determined by its fractional part: ϕ_m can therefore not be accurately determined because, among other reasons, the antennas are not truly

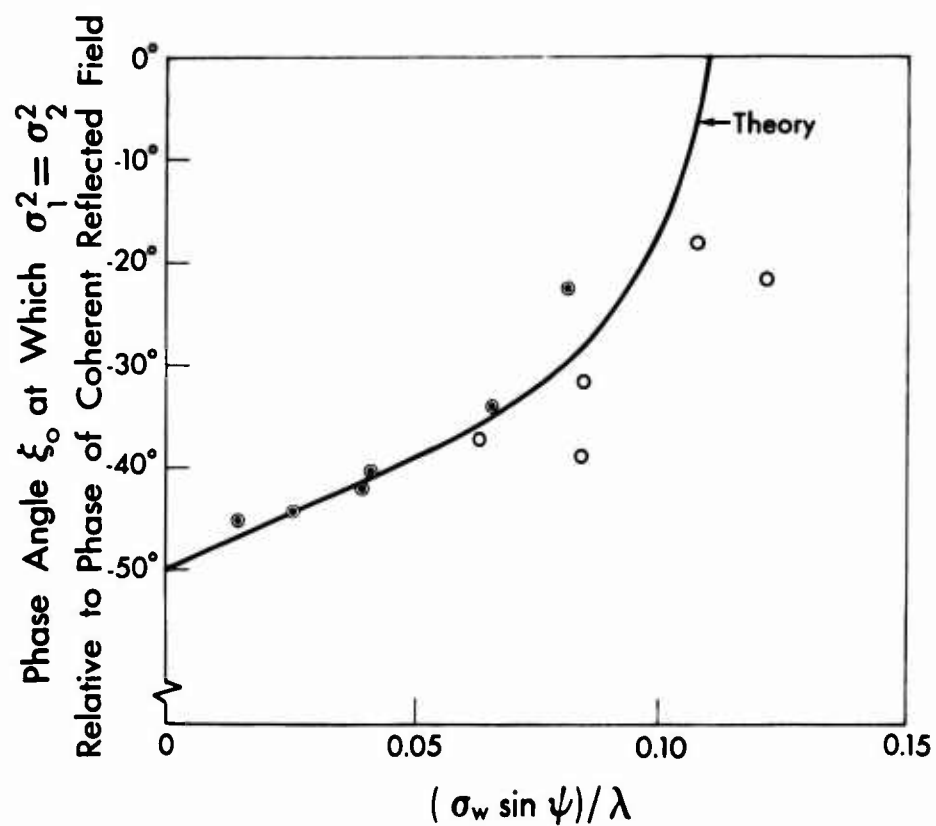


Fig. 8. Rotation of the variance ellipse. Experimental data by Beard (1965), theoretical curve computed by (57).

point sources and therefore D cannot be determined with the accuracy of a small fraction of a wavelength. However, this constant is additive and does not change with the water roughness σ_w , so that it simply represents a reference phase which does not affect the function $\xi_0(\sigma_w)$, except in shifting its plot up or down with respect to the origin. In plotting Figure 8, the additive constant ϕ_m was chosen so as to give the best fit with the experimental data. It can be seen that the theoretical curve calculated by (57) is in good agreement with the measured values shown in Figure 8. The orientation of the variance ellipse, as shown by both the theoretical analysis and the experimental data, rotates with varying σ_w ; this does not happen for plane-wave illumination and scatter; i.e., when transmitter and receiver are far apart and high above the rough surface (Fraunhofer scattering).

Good agreement is also obtained on comparing the theoretical formula (62), with ξ and η given by (49), with the experimental data shown in Figure 9. The experimental data are those reported by Beard (1967, Figure 16). The ordinate plots σ/C_0 , where C_0 is the amplitude of the smooth surface coherent component. The latter is a rather complicated function of the illuminated area and the gain function of the antennas (Beckmann and Spizzichino, 1963), but in this case represents simply a multiplicative constant which can be absorbed into n in (62), so that (62) has been plotted in Figure 9 with the multiplicative constant so chosen as to give the best fit to the measured data.

The extreme values σ_{\max}^2 , σ_{\min}^2 could be obtained by using (37) and substituting (60), (61) for σ_x^2 and σ_y^2 ; a less tedious method is to calculate K first and then to use the equations

$$\sigma_{\max}^2 + \sigma_{\min}^2 = \sigma^2, \quad \frac{\sigma_{\max}^2}{\sigma_{\min}^2} = K^2 \quad (86)$$

where the right sides are known from (62) and (66) respectively; on solving (86) one obtains

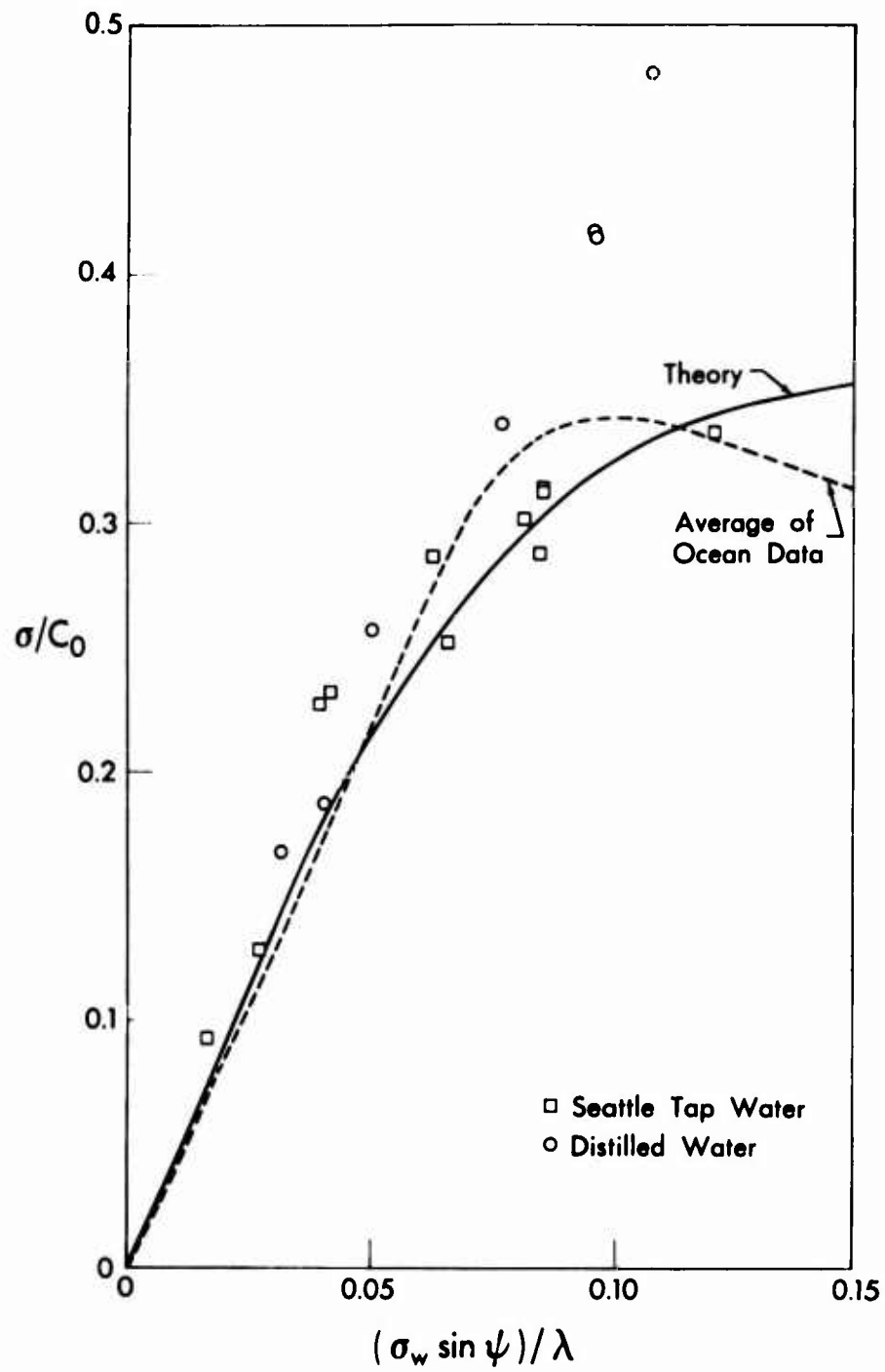


Fig. 9. RMS scattered amplitude. Experimental data by Beard (1966), theoretical curve computed by (62).

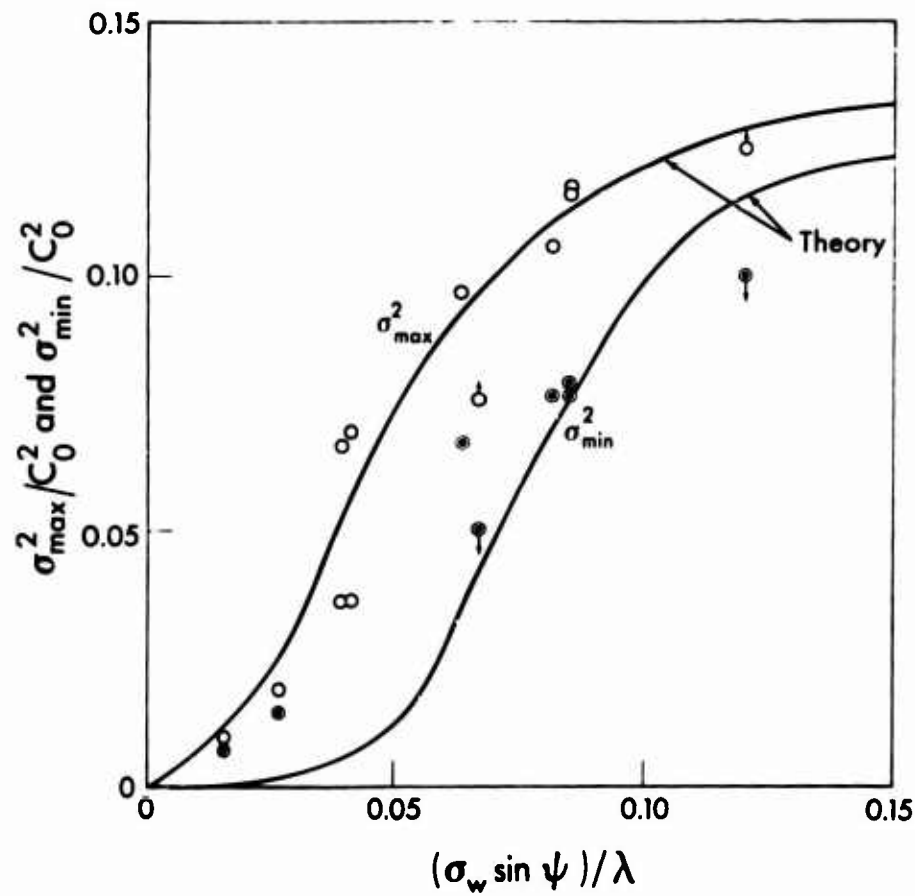


Fig. 10. Extreme values of the variance of the scattered field. Experimental data by Beard (1965), theoretical curve computed by (87).

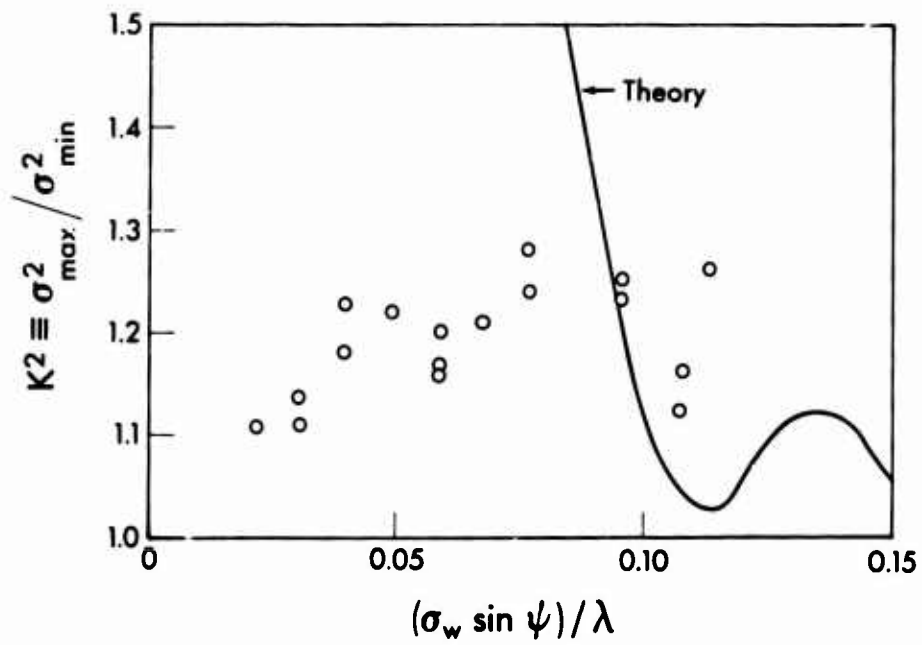


Fig. 11. Ratio of extreme variances of the scattered field. Experimental data by Beard (1966), theoretical curve computed by (66). For the reason of the discrepancy, see last paragraph of Section 4, p. 21.

$$\sigma_{\min}^2 = \frac{\sigma^2}{1 + K^2}$$

$$\sigma_{\max}^2 = K^2 \sigma_{\min}^2 \quad (87)$$

and these values, using the same multiplicative constant as in Figure 9, are plotted against the experimental data (Beard, 1965, Figure 34) in Figure 10.

Finally, Figure 11 shows a comparison of $K^2 = \sigma_{\max}^2 / \sigma_{\min}^2$ as calculated from (66) and (68) and as measured by Beard (1967, Figure 14). Although for large $(\sigma_w \sin \psi) / \lambda$ both theoretical and experimental data approach unity, there is not even qualitative agreement between theory and experiment for $\sigma_w \rightarrow 0$. The reason for this discrepancy, as has already been mentioned in the remarks following (74), is that for $\sigma_w \rightarrow 0$, the variance ellipse shrinks to a point; the ratio $K^2 = \sigma_{\max}^2 / \sigma_{\min}^2$ is then given by the limit of an indeterminate expression $0/0$, which can be resolved only after the second application of L'Hôpital's rule, yielding a critically sensitive value, which can obviously not be reproduced by a theory using approximations such as those used in the above analysis (neglection of lateral scattering, asymptotic methods approximating integrals, Newton's method approximating the location of the saddle point, etc.).

7. CONCLUSION

The theory developed in Sections 2 through 5 leads to qualitative agreement with, and provides insight into, the experimental measurements of the phase-quadrature components scattered by a random rough surface as performed by Beard (1965, 1967). The theory takes into account the finite distance between transmitter and receiver; i.e., the sphericity of the incident and scattered waves by using a hybrid geometrical-physical-optics approach and leads to a complicated phase distribution of the scattered field. The latter is calculated by use of simplifying assumptions and approximate integrations. Unlike the case of plane-wave illumination and reception in the Fraunhofer zone, the case under investigation

leads to asymmetrical phase distributions even if the rough surface is symmetrically distributed, and to a rotation of the variance ellipse with increasing roughness. Mathematically, these complications are reflected in the quantities in the fact that the quantities describing the scattered field are determined not by the exponential functions appearing in plane-wave scattering, but by confluent hypergeometric functions.

APPENDIX

The Confluent Hypergeometric Function ${}_1F_1\left(\frac{1}{2}; \frac{3}{2}; x\right)$

The quantities of interest associated with the scattered field are in this report expressed in terms of the confluent hypergeometric function

$$\begin{aligned}
 {}_1F_1\left(\frac{1}{2}; \frac{3}{2}; x\right) &= 1 + \frac{\frac{1}{2}}{\frac{3}{2}} x + \frac{\frac{1}{2} \cdot \frac{3}{2}}{\frac{3}{2} \cdot \frac{5}{2}} \frac{x^2}{2!} + \frac{\frac{1}{2} \cdot \frac{3}{2} \cdot \frac{5}{2}}{\frac{3}{2} \cdot \frac{5}{2} \cdot \frac{7}{2}} \frac{x^3}{3!} + \dots \\
 &= 1 + \frac{1}{3} x + \frac{1}{10} x^2 + \frac{1}{42} x^3 + \frac{1}{216} x^4 + \dots
 \end{aligned}$$

which is easily programmed on a digital computer. However, for quick information computations, a short table of ${}_1F_1\left(\frac{1}{2}; \frac{3}{2}; x\right)$ is included here, since tables of this function (Airey, 1926, 1927) are not readily accessible.

TABLE 1-A

x	${}_1F_1\left(\frac{1}{2}; \frac{3}{2}; x\right)$	x	${}_1F_1\left(\frac{1}{2}; \frac{3}{2}; x\right)$
0.00	1.00000	1.1	1.52757
0.02	1.00671	1.2	1.59700
0.04	1.01349	1.3	1.67129
0.06	1.02037	1.4	1.75083
0.08	1.02732	1.5	1.83603
0.10	1.03436	1.6	1.92736
0.15	1.05233	1.7	2.02531
0.20	1.07086	1.8	2.13041
0.25	1.08997	1.9	2.24325
0.30	1.10968	2.0	2.36445
0.35	1.13001	2.2	2.63478
0.40	1.15098	2.4	2.94764
0.45	1.17262	2.6	3.31041
0.50	1.19496	2.8	3.73183
		3.0	4.22221
0.55	1.21801	3.5	5.83596
0.60	1.24818	4.0	8.22631
0.65	1.26638	4.5	11.7973
0.70	1.29175	5.0	17.1722
0.75	1.31796	5.5	25.3164
0.80	1.34503	6.0	37.7301
0.85	1.37300	6.5	56.7504
0.90	1.40191	7.0	86.0296
0.95	1.43178	7.5	131.289
1.00	1.46265	8.0	201.510

REFERENCES

- Airey, J. R., "The confluent hypergeometric function," British Association Reports, pp. 276-294, Oxford, 1926; pp. 220-224, Leeds, 1927.
- Beard, C. I., "Preliminary results of phase-quadrature components of microwave forward scattering from random water waves," Boeing Document D1-82-0440, June 1965.
- Beard, C. I., "Behavior of non-Rayleigh statistics of microwave forward scatter from a random water surface," IEEE Trans. Antennas and Propagation AP-15, 649-657, September 1967; also, Boeing Document D1-82-0587, December 1966.
- Beckmann, P., "Statistical distribution of the amplitude and phase of a multiply scattered field," J. Res. NBS 66D, 231-240, 1962.
- Beckmann, P., "Probability in communication engineering," Harcourt, Brace & World, New York, 1967.
- Beckmann, P., and A. M. Spizzichino, "The scattering of electromagnetic waves from rough surfaces," Pergamon, London, and MacMillan, New York, 1963.
- Clarke, R. H., and G. O. Hendry, "Prediction and measurement of the coherent and incoherent power reflected from a rough surface," Trans. IEEE Antennas and Propagation AP-12, 353-363, May 1964.
- Stoker, J. J., "Water waves," Interscience, London-New York, 1957.